Virologica Sinica 39 (2024) 632–644

Contents lists available at ScienceDirect

Virologica Sinica

journal homepage: www.keaipublishing.com/en/journals/virologica-sinica
www.virosin.org

Research Article

AIMP2 restricts EV71 replication by recruiting SMURF2 to promote the degradation of 3D polymerase

Junrui Ren [a,1], Lei Yu [a,b,1], Qiuhan Zhang [a,b], Pengyu Ren [a], Yumeng Cai [a], Xueyun Wang [a], Ke Lan [a,b,c,*], Shuwen Wu [a,*]

[a] State Key Laboratory of Virology, College of Life Sciences, Wuhan University, Wuhan, 430072, China
[b] Medical Research Institute, Wuhan University, Wuhan, 430072, China
[c] Taikang Center for Life and Medical Sciences, Wuhan University, Wuhan, 430072, China

ARTICLE INFO

Keywords:
AIMP2
Enterovirus 71 (EV71)
3D polymerase
E3 ligase SMURF2
Ubiquitination

ABSTRACT

Hand, foot and mouth disease (HFMD), mainly caused by enterovirus 71 (EV71), has frequently occurred in the Asia-Pacific region, posing a significant threat to the health of infants and young children. Therefore, research on the infection mechanism and pathogenicity of enteroviruses is increasingly becoming important. The 3D polymerase, as the most critical RNA-dependent RNA polymerase (RdRp) for EV71 replication, is widely targeted to inhibit EV71 infection. In this study, we identified a novel host protein, AIMP2, capable of binding to 3D polymerase and inhibiting EV71 infection. Subsequent investigations revealed that AIMP2 recruits the E3 ligase SMURF2, which mediates the polyubiquitination and degradation of 3D polymerase. Furthermore, the antiviral effect of AIMP2 extended to the CVA16 and CVB1 serotypes. Our research has uncovered the dynamic regulatory function of AIMP2 during EV71 infection, revealing a novel antiviral mechanism and providing new insights for the development of antienteroviral therapeutic strategies.

1. Introduction

Enterovirus 71 (EV71) is a positive-sense single-stranded RNA virus belonging to the *Picornaviridae* family. It lacks envelope and protrusions, making it one of the simplest viruses (Baggen et al., 2018; Solomon et al., 2010). The virus was first isolated from the stool of a female infant with HFMD in California, USA (Schmidt et al., 1974). EV71 typically causes large-scale outbreaks of hand, foot and mouth disease (HFMD), and primarily affects children. The main clinical symptoms include fever, a blister-like rash on hands and feet (Cox and Levent, 2018; Ooi et al., 2010; Saguil et al., 2019). In severe cases, it can lead to central nervous system damage, aseptic meningitis, brainstem encephalitis, and other diseases (Hu et al., 2015; You et al., 2023). Due to the significant public health impact, enteroviruses have attracted increasing attention around the world.

The genome of EV71 comprises two noncoding regions (a 5′UTR and a 3′UTR) as well as one coding region. EV71 5′UTR contains an internal ribosomal entry site (IRES) and multiple stem loops that can recruit numerous IRES trans-acting factors (ITAFs) mediating the initiation of viral capsid-independent protein synthesis (Hagiwara et al., 1984). The coding region is generally considered to encode an open reading frame (ORF), which is translated into a long polypeptide and then progressively cleaved into four structural proteins (VP1, VP2, VP3 and VP4) and seven nonstructural proteins (2A, 2B, 2C, 3A, 3B, 3C and 3D). These different proteins coordinate to promote the proliferation of EV71 and mutations of these viral proteins may affect the virus's virulence (Ang et al., 2021; Wang and Li, 2019; Xia et al., 2015; Yuan et al., 2018). The 3D protein functions as an RNA-dependent RNA polymerase (RdRp), directly utilizing the viral genomic RNA as a template to synthesize minus-strand RNA, forming double-stranded RNA (dsRNA), and subsequently participating in the synthesis of viral genomes and proteins, which play crucial roles in viral replication (Zhang et al., 2021). Recent research has revealed the presence of another ORF, which encodes the viral protein ORF2p and can impact virus infection (Guo et al., 2019; Lulla et al., 2019).

Aminoacyl-tRNA synthetase interacting multifunctional protein 2 (AIMP2), also known as JTV1 or p38, is a component of the multi-synthetase complexes (MSCs). It is primarily involved in intracellular

* Corresponding authors.
E-mail addresses: shuwenwu@whu.edu.cn (S. Wu), klan@whu.edu.cn (K. Lan).
[1] Junrui Ren and Lei Yu contributed equally to this work.

https://doi.org/10.1016/j.virs.2024.06.009
Received 19 March 2024; Accepted 25 June 2024
Available online 28 June 2024
1995-820X/© 2024 The Authors. Publishing services by Elsevier B.V. on behalf of KeAi Communications Co. Ltd. This is an open access article under the CC BY-NC-ND license (http://creativecommons.org/licenses/by-nc-nd/4.0/).

proteins synthesis (Nechushtan et al., 2009; Ofir-Birin et al., 2013). AIMP2 has several roles in tumorigenesis. Its excessive accumulation can accelerate the formation of Parkinson's disease, while it can also suppress the occurrence of gastric and colorectal cancers by negatively regulating Wnt/β-catenin signaling (Kim et al., 2011; Shin et al., 2022; Yum et al., 2016). Several studies have demonstrated that AIMP2 acts as a multifaceted tumor suppressor by regulating target proteins through ubiquitin-mediated degradation pathways. AIMP2 directly interacts with p53, preventing its degradation mediated by MDM2-linked ubiquitination (Han et al., 2008). Additionally, it promotes apoptosis by down-regulating TNF receptor-associated factor 2 (TRAF2) through the ubiquitin pathway (Choi et al., 2009a). Heterozygous mice with low AIMP2 expression exhibit increased tumor susceptibility (Choi et al., 2009b). However, the function of AIMP2 in viral infection has rarely been studied, and its role during EV71 infection remains unclear.

In this study, we found that AIMP2 plays a negative regulatory role in EV71 infection by recruiting the E3 ligase SMURF2 to promote the degradation of 3D polymerase, thereby inhibiting EV71 genome replication. This antiviral effect also extends to enterovirus serotypes CVA16 and CVB1. Our findings suggest that AIMP2 affects EV71 replication by regulating the ubiquitination of 3D polymerase, presenting a new potential target for antiviral therapy.

2. Materials and methods

2.1. Cells and viruses

The human rhabdomyosarcoma (RD) cells, Vero cells (African green monkey kidney cells), Human HEK293T cells and HeLa cells were cultured in Dulbecco's modified Eagle's medium (DMEM, Biological Industries, Israel) supplemented with 10% fetal bovine serum (FBS, Biological Industries) and 1% antibiotics (penicillin and streptomycin, Gibco, USA). All cell lines were derived from our laboratory and grown at 37 °C and 5% CO_2. The EV71 (JX678881.1), CVA16 (KM516102.1) and CVB1 (JX976769.1) strains were obtained from the State Key Laboratory of Virology, Wuhan University. All viruses were propagated with RD cells and viral titers were determined by plaque assay.

2.2. Antibodies and reagents

In this study, the following antibodies were used: anti-AIMP2 rabbit polyclonal antibody (Proteintech, 10424-1-AP, USA), anti-SMURF2 rabbit monoclonal antibody (ABclonal, A2278, China), anti-EV71 VP1 mouse monoclonal antibody (Abcam, ab169442, England), anti-EV71 3D mouse monoclonal antibody (GenTex, GTX630193, USA), anti-dsRNA rJ2 monoclonal antibody (Millipore, MABE1134, USA), anti-Flag antibody (Sigma, F1804, USA), anti-HA antibody (Sigma, H6908, USA), anti-Myc antibody (ABclonal, AE070, China), anti-α-Tubulin mouse monoclonal antibody (Sigma, T6199, USA), anti-GAPDH rabbit monoclonal antibody (ABclonal, AC033, China), anti-Vinculin rabbit monoclonal antibody (ABclonal, A2752, China), HRP-conjugated goat anti-mouse or anti-rabbit IgG (Jackson Immunology Research Laboratories, 115-035-174 and 111-005-144, USA), goat anti-mouse or anti-rabbit antibodies conjugated with Alexa Fluor 488 and 555 (Thermo Fisher Scientific, A-11001 and A-21422, USA). The main reagents used were as follows: anti-Flag M2 beads (Sigma, A2220), recombinant protein A agarose (Thermo Fisher Scientific, 15948-014, USA), recombinant protein G agarose (Thermo Fisher Scientific, 15920-010, USA), cycloheximide (CHX) (MedChemExpress, HY-12320, USA), MG132 (MedChemExpress, HY-13259, USA), chloroquine (CQ) (MedChemExpress, HY-17589A, USA), 3-Methyladenine (3MA) (MedChemExpress, HY-19312, USA), protease inhibitor cocktail (Sigma, P8340, USA), Opti-MEM (Invitrogen, USA), Neofect™ DNA transfection reagent (NEOFECT, TF20121201, China), BOLG-RNA™ reagent (BIOLOGY, BOLG101, China), Dual luciferase reporter assay kit (Promega, E1980, USA).

2.3. Plasmid construction

Total RNA was extracted from HEK293T cells and reverse transcribed to cDNA, and the genes encoding human AIMP2 and SMURF2 were amplified from cDNA library by PCR with specific primers. The cDNA encoding AIMP2 was cloned into the *Eco*RI/*Bam*HI site of pCDH-CMV-SF-IRES-Blast and the *Eco*RI/*Xho*lI site of pCMV-HA, respectively. The cDNA encoding SMURF2 was cloned into the *Eco*RI/*Bam*HI site of pCDH-CMV-SF-IRES-Blast and the *Bam*HI/*Hin*dlII site of pCMV-Myc. The EV71 *3C* gene was amplified by PCR from the pACYC-EV-A71-FL plasmid containing the full-length cDNA of EV71, which was donated by Prof. Bo Zhang (Wuhan Institute of Virology, Chinese Academy of Sciences) (Shang et al., 2013). The PCR products were inserted into the p3×Flag-CMV-14 vector at *Eco*RI and *Bam*HI sites. The EV71 3D plasmids, 2C plasmids, pRK-Myc-Ub-WT, pRK-Myc-Ub-K48 and pRK-Myc-Ub-K63 were derived from the plasmid library in our laboratory. Plasmids transfection was performed using polyethylenimine or Neofect™ DNA transfection reagent according to the manufacturer's instructions.

2.4. Western blotting and coimmunoprecipitation

Cells were transfected with indicated plasmids for 36–48 h, and then they were lysed in Western and IP lysis buffer (Beyotime) supplemented with protease inhibitor cocktail and PMSF at 4 °C for 1 h. Cell debris was centrifuged at 13,400 ×*g* for 15 min at 4 °C and the supernatant was collected. Ten percent of the samples were used as an input control. The remaining lysate was immunoprecipitated with M2 affinity beads or corresponding antibodies overnight at 4 °C. The beads were washed with lysis buffer for three times, resuspended in 30 μL 2×SDS loading buffer and boiled at 100 °C for 10 min. The samples were separated on SDS-PAGE and transferred to nitrocellulose membranes (Bio-Rad Laboratories). The membranes were incubated with the indicated antibodies overnight at 4 °C and then detected with the HRP-conjugated secondary antibodies.

2.5. Quantitative real-time PCR

Cells were collected and lysed using TRIzol reagent (Ambion, USA), and the total cellular RNA was extracted according to standard instructions. The RNA was reverse transcribed into cDNA using HiScript III RT Super Mix (Vazyme, China). The cDNA mixture was then diluted 10-fold and qPCR was performed using SYBR green qPCR master mix (Vazyme, China) to analyze the RNA levels of the target genes. The relative abundance of target RNA and viral RNA were analyzed by the $2^{-\Delta\Delta CT}$ method and normalized using the housekeeping gene *GAPDH*.

The titer of EV71 virus in the supernatant was analyzed by absolute quantification. The EV71 genome in the supernatant was extracted with Viral Nucleic Acid Isolation Kit (Simgen), the vRNA was reverse transcribed using HiScript III RT Super Mix (Vazyme), and the plasmid pACYC-EV-A71-FL was used as a standard sample to draw the standard curve. The copy number was calculated according to the standard curve. All qPCR primer sequences used in the study are listed in Supplementary Table S1.

2.6. Plaque assay

Plaque assays were performed according to the protocol previously described (Baer and Kehn-Hall, 2014). RD cells were seeded in 12-well plates one day in advance and cultured in an incubator until cell density reached 90%–100%. The cells were then infected with a series of 10-fold dilutions of virus for 1 h at 37 °C, washed once with PBS and covered with the agarose mixture (low melting point agarose, 2×MEM, 2% fetal bovine serum). After agarose had solidified, the cells were incubated with the virus for another 48 h. They were then fixed with 4%

paraformaldehyde and stained with 1% crystal violet. Virus titers were determined based on the number of plaques.

2.7. Immunofluorescence microscopy

Cells were seeded onto coverslips of 24-well plates for transfection as indicated. After 24 h, cells were fixed with 4% paraformaldehyde for 30 min or infected with virus at an MOI of 1 for 12 h before fixation. Cells were permeabilized with 0.2% Triton-X 100 for 15 min and then blocked with 5% bovine serum albumin (BSA) for 1 h at 26 °C, followed by incubation with the specific primary antibodies at 4 °C overnight. Subsequently, the cells were stained with the indicated fluorescent secondary antibodies for 1 h at 26 °C. Nuclei were stained with DAPI (Beyotime) for 10 min, and finally images were analyzed using fluorescence microscopy.

2.8. RNA interference

HEK293T/RD cells were transfected with a negative control siRNA or one of two siRNA against the target gene using BOLG-RNA™ reagent according to the manufacturer's instructions. Cells were harvested after 36 h of transfection and assessed for RNA interference efficiency using immunoblotting or RT-qPCR. All siRNA sequences used in the experiments are listed in Supplementary Table S1.

2.9. EV71 attachment and entry assay

For virus attachment assays, cells were infected with EV71 at an MOI of 3. After treatment at 4 °C for 1 h, the cells were washed twice with PBS, and cell lysates were collected for analysis of viral RNA by RT-qPCR. For the entry assays, the cells were incubated for 1 h at 4 °C after virus infection, and the cells were washed twice with PBS. The cells were then incubated at 37 °C for 1 h. Cellular RNA was extracted and viral RNA was analyzed by RT-qPCR.

2.10. Dual-luciferase reporter assay

The plasmid pRHF-EV-A71-5′UTR was constructed as previously described to evaluate the IRES-driven translational activity of EV71 (Tang et al., 2020; Zhang et al., 2015). The plasmids were transfected into HEK293T cells according to the instructions, and the plasmid pRL-TK expressing Renilla luciferase was used as a control. Cell lysates were collected after 36 h of transfection to detect luciferase activities using Dual luciferase reporter assay kit (Promega).

2.11. Ubiquitination assay

HEK293T cells were transfected with the indicated plasmids for 36 h and then treated with DMSO or MG132 (20 μM) for another 12 h. Cells lysates were subjected to immunoprecipitation with the indicated antibodies. The protein level was then measured by Western blotting.

2.12. Protein stability assay

HEK293T cells were transfected with indicated plasmids. After 36 h of incubation, the cells were treated with 100 μg/mL cycloheximide (CHX) for indicated time. Cells were collected and lysed for immunoblot analysis. The intensity of each band of 3D polymerase was normalized to Tubulin protein intensity.

2.13. Statistical analysis

The data were analyzed by unpaired Student *t*-test. Statistical results were analyzed using Prism GraphPad 8. The data were shown as the mean ± standard deviation (SD) from three independent experiments. *P* value < 0.05 means significant (*, $P < 0.05$; **, $P < 0.01$; ***, $P < 0.001$; ****, $P < 0.0001$), *P* value > 0.05 means no significant (NS).

3. Results

3.1. AIMP2 mRNA and protein level was downregulated during EV71 infection

To identify host proteins crucial for disrupting or antagonizing EV71 infection, we analyzed bulk RNA-seq data from the GEO public database (GSE103308), and found that AIMP2 RNA levels were significantly downregulated during EV71 infection (Fig. 1A). We thus speculated that AIMP2 may play a role in EV71 infection. First, we infected RD cells with EV71 (MOI = 1) and harvested the cells at the indicated time points to assess AIMP2 RNA levels via RT-qPCR and AIMP2 protein levels via immunoblotting (Fig. 1B and C). Consistent with the results of the database analysis, AIMP2 expression decreased under EV71 infection conditions. To determine whether this phenomenon is cell-specific, we repeated the infection experiments in Vero cells, where the degradation of AIMP2 was also observed, suggesting that the downregulation of AIMP2 is not cell-specific (Fig. 1D). These results suggest that AIMP2 is downregulated during EV71 infection.

3.2. Overexpression of AIMP2 inhibits EV71 infection

AIMP2 have been previously identified as a component of MSCs, primarily involved in protein synthesis. However, an increasing number of studies have shown that AIMP2 can function as a tumor suppressor, regulating the development of cancer and tumors (Nechushtan et al., 2009). Previous studies have indicated that AIMP2 can be downregulated during EV71 infection. Thus, to investigate the role of AIMP2 in EV71 infection, Vero or RD cells were transfected with increasing amounts of the AIMP2-Flag plasmid and subsequently infected with EV71 (MOI = 1). Western blot analysis was performed to determine tEV71 protein levels, and we found that the expression of VP1 gradually decreased with increasing AIMP2 plasmid dosage (Fig. 2A and C). RT-qPCR analysis was performed to determine EV71 RNA levels, showing a similar gradual decrease in EV71 RNA levels in Vero cells with increasing AIMP2 plasmid dosage (Fig. 2B). The above results indicate that overexpression of AIMP2 inhibits EV71 infection in a dose-dependent manner. We also observed a significant reduction in the intensity of green fluorescence in Vero cells by immunofluorescence staining, suggesting that the number of EV71 virions was reduced in the presence of AIMP2 (Fig. 2D). To further validate the role of AIMP2 in EV71 infection, RD cells were transfected with the AIMP2-Flag plasmid and were then treated with EV71 at an MOI of 0.1 for 0–36 h. Western blot and RT-qPCR analyses indicated that AIMP2 overexpression reduced the intracellular EV71 protein levels (Fig. 2E) and RNA transcript levels (Fig. 2F), and the EV71 genome copy number in the supernatant (Fig. 2G). Moreover, we analyzed the viral plaque formation, and found that viral plaque formation was reduced in AIMP2-overexpressing cells compared to control cells (Fig. 2H). Immunofluorescence analysis revealed that the intensity of green fluorescence was significantly reduced in RD cells transfected with the AIMP2-Flag plasmid (Fig. 2I). Taken together, these results suggest that overexpression of AIMP2 inhibits EV71 replication.

3.3. Knockdown of AIMP2 promotes EV71 infection

Since AIMP2 overexpression plays a negative regulatory role in EV71 infection, we hypothesized that AIMP2 knockdown facilitates EV71 infection. First, endogenous AIMP2 was knockdown in RD cells via siRNA, and the knockdown efficiency was assessed via RT-qPCR and Western blotting. Both siRNAs targeting AIMP2 effectively reduced the intracellular AIMP2 RNA transcript level by 78% and 90% (Fig. 3A), and

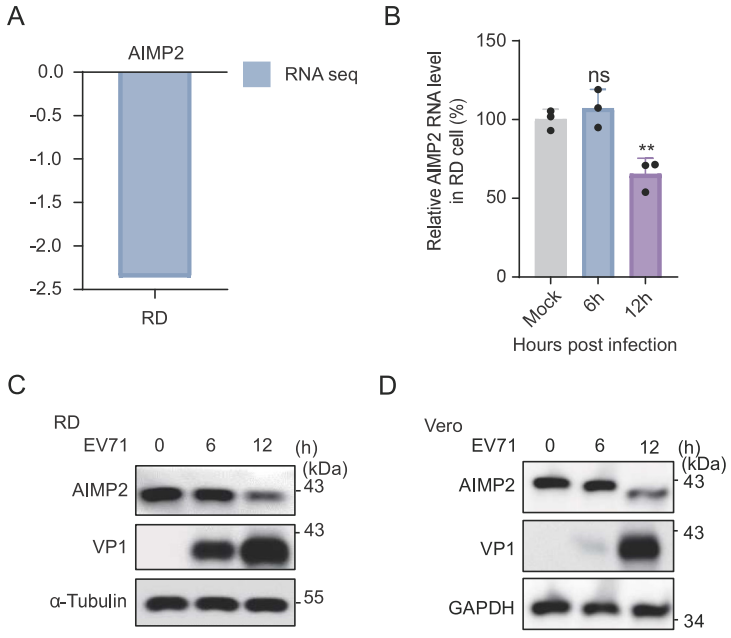

Fig. 1. AIMP2 mRNA and protein levels were downregulated during EV71 infection. **A** Analyze the changes in AIMP2 RNA levels under EV71 infection status in the GEO database (GSE103308). **B–D** RD or Vero cells infected with EV71 (MOI = 1) for the indicated times. The EV71 VP1 and AIMP2 protein levels were measured by Western blotting (**C and D**), and the relative EV71 RNA levels were determined by RT-qPCR, and normalized to those of GAPDH (**B**). The results represent the means ± SD from three independent experiments. Statistical significance was analyzed using Student's *t*-test (**$P < 0.01$; ns, not significant). MOI, multiplicity of infection.

decreased the AIMP2 protein level by 67% and 82% (Fig. 3B) compared to the non-targeting control (NC) group. Next, RD cells were incubated with EV71 (MOI = 1) for 0–12 h. The intracellular protein and RNA levels were measured, and the EV71 VP1 protein (Fig. 3C) and RNA levels (Fig. 3D) were significantly increased by transfection of the indicated siRNAs compared to those in the NC group. We further investigated EV71 genome copy number in the supernatant along with the plaque formation ability of EV71. Titer determination indicated that AIMP2 knockdown increased the extracellular viral titer (Fig. 3E), and the number of plaque-forming units also increased after AIMP2 knockdown (Fig. 3F). Furthermore, immunofluorescence analysis revealed that the intensity of green fluorescence was significantly increased in RD cells transfected with the indicated siRNAs (Fig. 3G). Taken together, these results suggest that AIMP2 knockdown effectively facilitates EV71 infection.

3.4. AIMP2 affects the replication of EV71, but does not affect the attachment, entry and translation of EV71

Many studies have demonstrated that the antagonistic effects of host proteins on viral infection are mediated primarily through interference with the viral life cycle (Lin et al., 2009; Shih et al., 2011). To determine the specific stage of the EV71 life cycle is affected by AIMP2, we conducted an assessment of EV71's attachment, entry, replication and translation. For the attachment and entry assays, RD cells were transfected with the AIMP2-Flag plasmid, and incubated with EV71 at an MOI of 3 at 4 °C for 1 h (attachment assay). Subsequently, the cells were infected with EV71 by incubation at 37 °C for 1 h (entry assay). RD cells were subjected to the same treatment after AIMP2 was knocked down. Evaluation of the attachment and entry steps by RT-qPCR revealed that neither overexpression nor knockdown of AIMP2 resulted in significant differences in viral attachment (Fig. 4A and B) or entry (Fig. 4C and D) compared to the NC group.

To further explore whether AIMP2 affects IRES-mediated viral RNA translation, a bicistronic luciferase reporter system containing the 5′UTR of the EV71 genome was employed. This system facilitated the expression of firefly luciferase (Fluc), while Renilla luciferase (RLuc) served as a control for translational activity. The ratio of FLuc to RLuc (FLuc/RLuc) represents the ability of AIMP2 to modulate IRES-mediated translation initiation (Li and Brewer, 2020; Lin et al., 2009). HEK293T cells were transfected with both the AIMP2-Flag plasmid and the bicistronic plasmids for 36 h. Afterwards, the cells were lysed, and luciferase activity was assayed. Cell lysates were also subjected to Western blot analysis (Fig. 4E). Similarly, HEK293T cells were transfected with the dual-luciferase plasmids after the knockdown of endogenous AIMP2. Cell lysates were then collected and analyzed (Fig. 4F). The results revealed that neither overexpression nor knockdown of AIMP2 significantly affected IRES-mediated translational activity.

To evaluate the replication step, we measured the fluorescence intensity of dsRNA synthesized during EV71 replication. Using immunofluorescence analysis, we found that the fluorescence intensity of dsRNA (green fluorescence) was significantly greater compared to the control cells after AIMP2 knockdown (Fig. 4G). The relative abundance of dsRNA and DAPI staining was quantified using Image J software (Fig. 4H). Taken together, these results indicate that AIMP2 affects the replication step of EV71 life cycle.

3.5. AIMP2 interacts with EV71 3D polymerase

In the above study, we found that AIMP2 influenced EV71 replication. Given that the EV71 3D protein is a crucial RdRp for viral replication, we speculated that might AIMP2 inhibit EV71 replication by

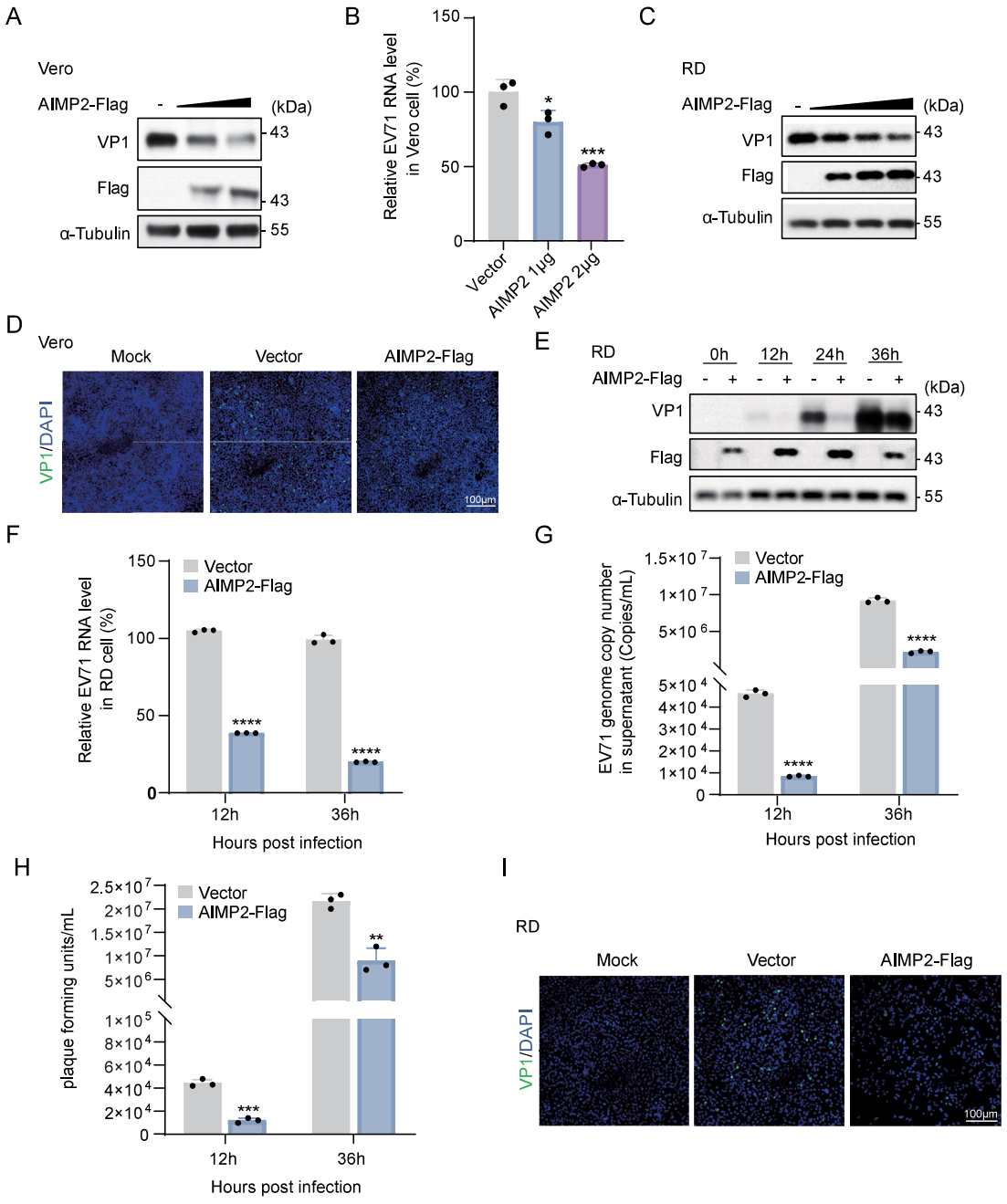

Fig. 2. Overexpression of AIMP2 inhibits EV71 infection. **A, B** Vero cells were transfected with AIMP2-Flag plasmid (0, 1, or 2 μg) for 36 h, and were then infected with EV71 (MOI = 1) for 12 h. The EV71 VP1 and AIMP2 protein levels were measured by Western blotting using the indicated antibodies (**A**). The relative EV71 RNA levels were determined by RT-qPCR, and normalized to the level of GAPDH (**B**). **C** RD cells were transfected with increasing amounts of the AIMP2-Flag plasmid (0, 0.5, 1, or 2 μg) for 24 h and then infected with EV71 (MOI = 1) for 12 h. EV71 VP1 protein expression was then measured by Western blotting. **D** Vero cells were transfected with AIMP2-Flag for 24 h, infected with EV71 for 12 h and subjected to immunostaining with an anti-VP1 antibody (green) and staining with DAPI (blue). The presented images were acquired using fluorescence microscopy. Scale bars = 100 μm. **E** RD cells were transfected with the AIMP2-Flag plasmid and then infected with EV71 (MOI = 0.1) for the indicated times. The EV71 VP1 and AIMP2 protein levels were measured by Western blotting using the indicated antibodies. **F** The relative EV71 RNA levels were determined by RT-qPCR and normalized to the level of GAPDH. **G** The EV71 genome copy number in the supernatant was analyzed by RT-qPCR and calculated based on a standard curve. **H** EV71 in cell supernatants was evaluated by a plaque formation assay. **I** RD cells transfected with AIMP2-Flag plasmid were infected with EV71 (MOI = 1) for 12 h and then subjected to immunostaining for VP1 (green) and staining with DAPI (blue). The presented images were acquired using fluorescence microscopy. Scale bars = 100 μm. The results represent the means ± SD from three independent experiments. Statistical significance was analyzed using Student's *t*-test (*$P < 0.05$, **$P < 0.01$, ***$P < 0.001$, ****$P < 0.0001$). PFU, plaque-forming units.

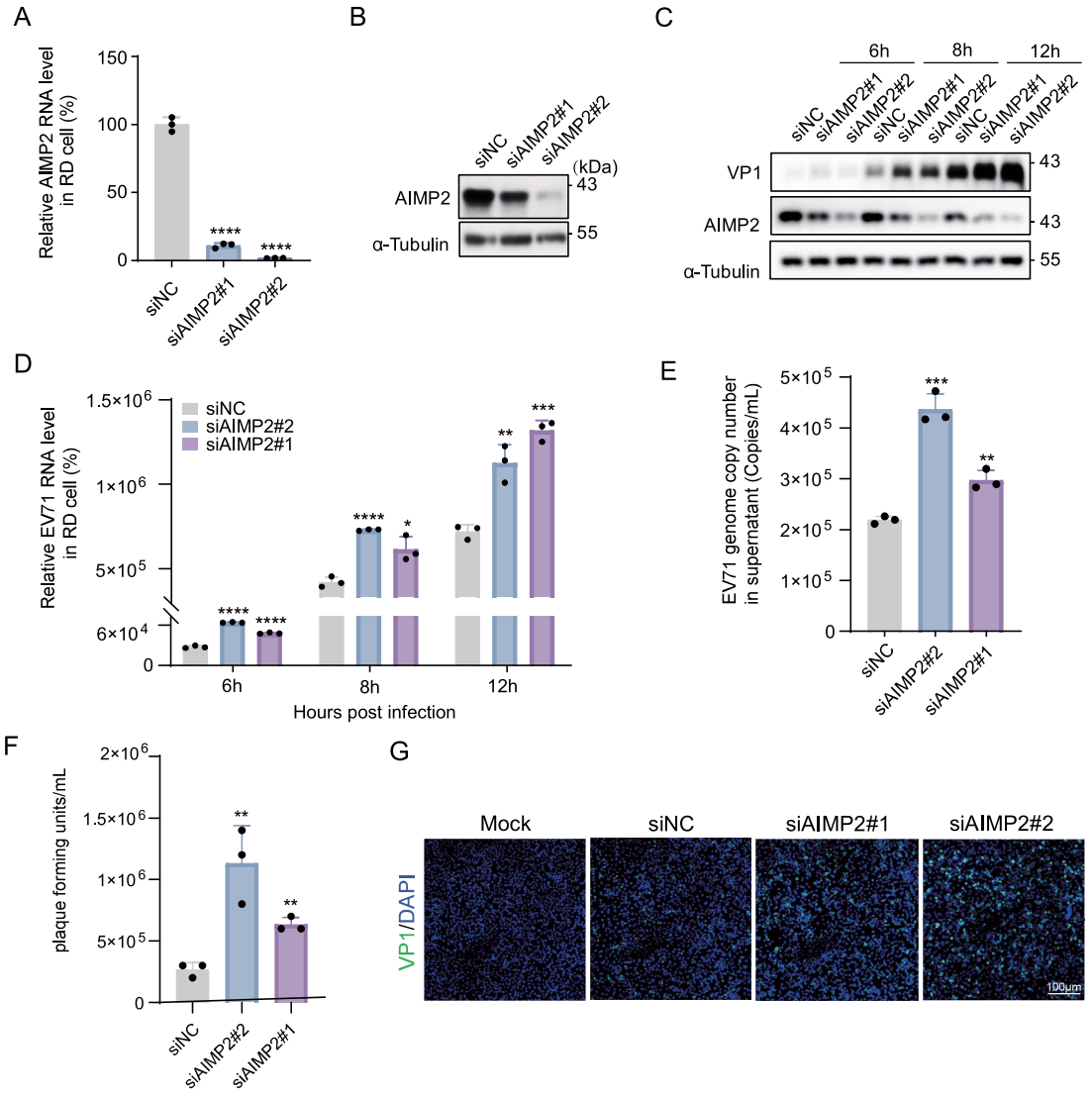

Fig. 3. Knockdown of AIMP2 promotes EV71 infection. **A, B** RD cells were transfected with a negative control siRNA or one of two siRNAs targeting human AIMP2, and after 36 h, the knockdown efficiency of AIMP2 was determined via RT-qPCR (**A**) and Western blot (**B**). **C** RD cells were transfected with control siRNA or one of two siRNAs targeting human AIMP2 for 24 h and were then infected with EV71 (MOI = 1) for the indicated times. The EV71 VP1 and AIMP2 protein levels were measured by Western blotting using the indicated antibodies. **D** The relative EV71 RNA levels in RD cells at the indicated times were determined by RT-qPCR and normalized to the level of GAPDH. **E** The EV71 genome copy number in the supernatant was analyzed by RT-qPCR and calculated based on a standard curve. **F** EV71 in cell supernatants was subjected to a plaque formation assay. **G** RD cells were transfected with AIMP2-Flag for 24 h, infected with EV71 (MOI = 1) for 12 h and subjected to immunostaining with an anti-VP1 antibody (green) and staining with DAPI (blue). The presentative images were acquired using fluorescence microscopy. Scale bars = 100 μm. The results represent the means ± SD from three independent experiments. Statistical significance was analyzed using Student's *t*-test (**$P < 0.01$, ***$P < 0.001$, ****$P < 0.0001$).

affecting 3D polymerase. To further explore this possibility, we performed exogenous coimmunoprecipitation assays. The results indicated that exogenous AIMP2 coimmunoprecipitated with 3D polymerase (Fig. 5A and B). We also investigated the potential interaction between AIMP2 and EV71 helicase 2C, but found no interaction between them (Supplementary Fig. S3). In addition, we performed an endogenous immunoprecipitation assay. In this assay, RD cells were not infected (Mock) or infected with EV71 at an MOI of 1 for 12 h, and then cell lysates were subjected to immunoprecipitation with an anti-AIMP2 antibody or control IgG. The results suggested that there was a significant interaction between AIMP2 and 3D polymerase during EV71 infection (Fig. 5C). To further verify the above results, we investigated whether AIMP2 and 3D polymerase are located in the same cellular compartment via confocal microscopy. The results indicate that exogenous AIMP2 and 3D polymerase were primarily colocalized in the cytoplasm (Fig. 5D). Additionally, endogenous AIMP2 and 3D polymerase were also colocalized in the same regions during EV71 infection (Fig. 5E). Taken together, these results demonstrate that AIMP2 interacts with 3D polymerase.

3.6. AIMP2 degrades 3D polymerase through the ubiquitin-proteasome pathway

The above results demonstrated that AIMP2 inhibits EV71 replication and interacts with 3D polymerase. We hypothesized that AIMP2 affects viral replication by influencing the stability of 3D polymerase. To test this

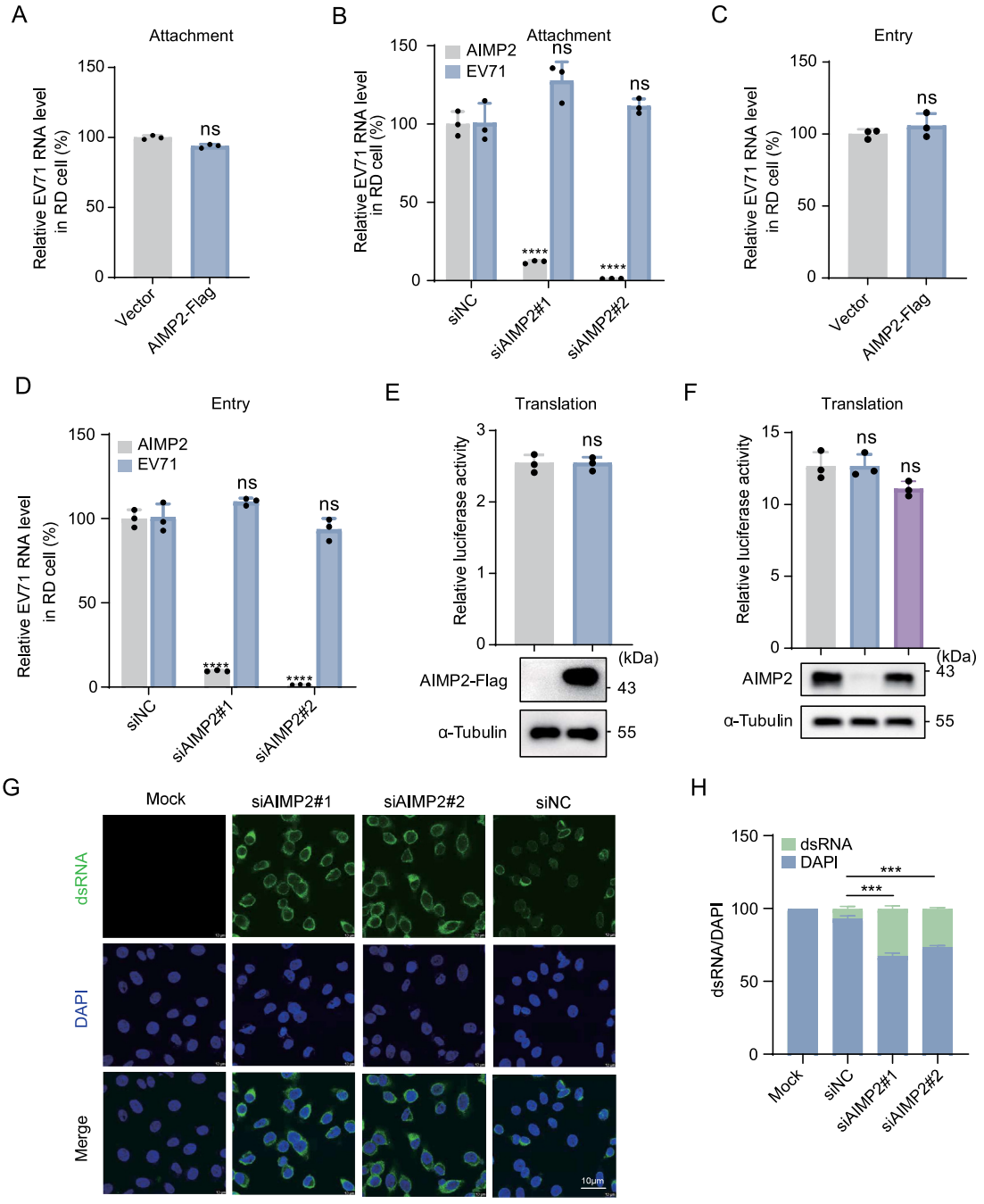

Fig. 4. AIMP2 affects the replication of EV71, does not affect the attachment, entry and translation of EV71. **A, C** RD cells were transfected with the AIMP2-Flag plasmid for 36 h and were then infected with EV71 (MOI = 3) for the indicated times. After treatment at 4 °C for 1 h (**A**) the cells were infected by incubation at 37 °C for another hour (**C**). Relative EV71 RNA levels were determined by RT-qPCR and normalized to the GAPDH RNA level. **B, D** RD cells were transfected with control siRNA or one of two siRNAs targeting human AIMP2 for 36 h and were then infected with EV71 (MOI = 3) for indicated times. After treatment at 4 °C for 1 h (**B**) the cells were infected by incubation at 37 °C for another hour (**D**). Relative EV71 RNA levels were determined by RT-qPCR and normalized to the GAPDH RNA level. **E** HEK293T cells were transfected with the AIMP2-Flag plasmid, 200 ng of pRHF-EV-A71 5′UTR and other plasmid DNA as indicated. After 36 h of transfection, the cells were lysed, and luciferase activity was analyzed. Cell lysates were also subjected to western blot analysis. **F** HEK293T cells were transfected with control siRNA or one of two siRNAs targeting human AIMP2 for 12 h and were then transfected with 200 ng of pRHF-EV71 5′UTR and other plasmid DNA as indicated. After 36 h transfection, the cells were lysed, and luciferase activity was analyzed. Cell lysates were also subjected to western blot analysis. **G** RD cells were transfected with control siRNA or one of two siRNAs targeting human AIMP2 for 36 h and were then infected with EV71 (MOI = 1) for 7 h. After treatment at 4 °C for 1 h, the cells were further incubated at 37 °C for 6 h. Uninfected cells served as controls. Then, the cells were fixed for immunostaining using an anti-dsRNA rJ2 monoclonal antibody (green), and nuclei were labeled with DAPI (blue). Scale bars = 10 μm. **H** The dsRNA/DAPI ratio was quantified using ImageJ software (n = 3). The results represent the means ± SD from three independent experiments. Statistical significance was analyzed using Student's *t*-test (***$P < 0.001$, ****$P < 0.0001$; ns, not significant).

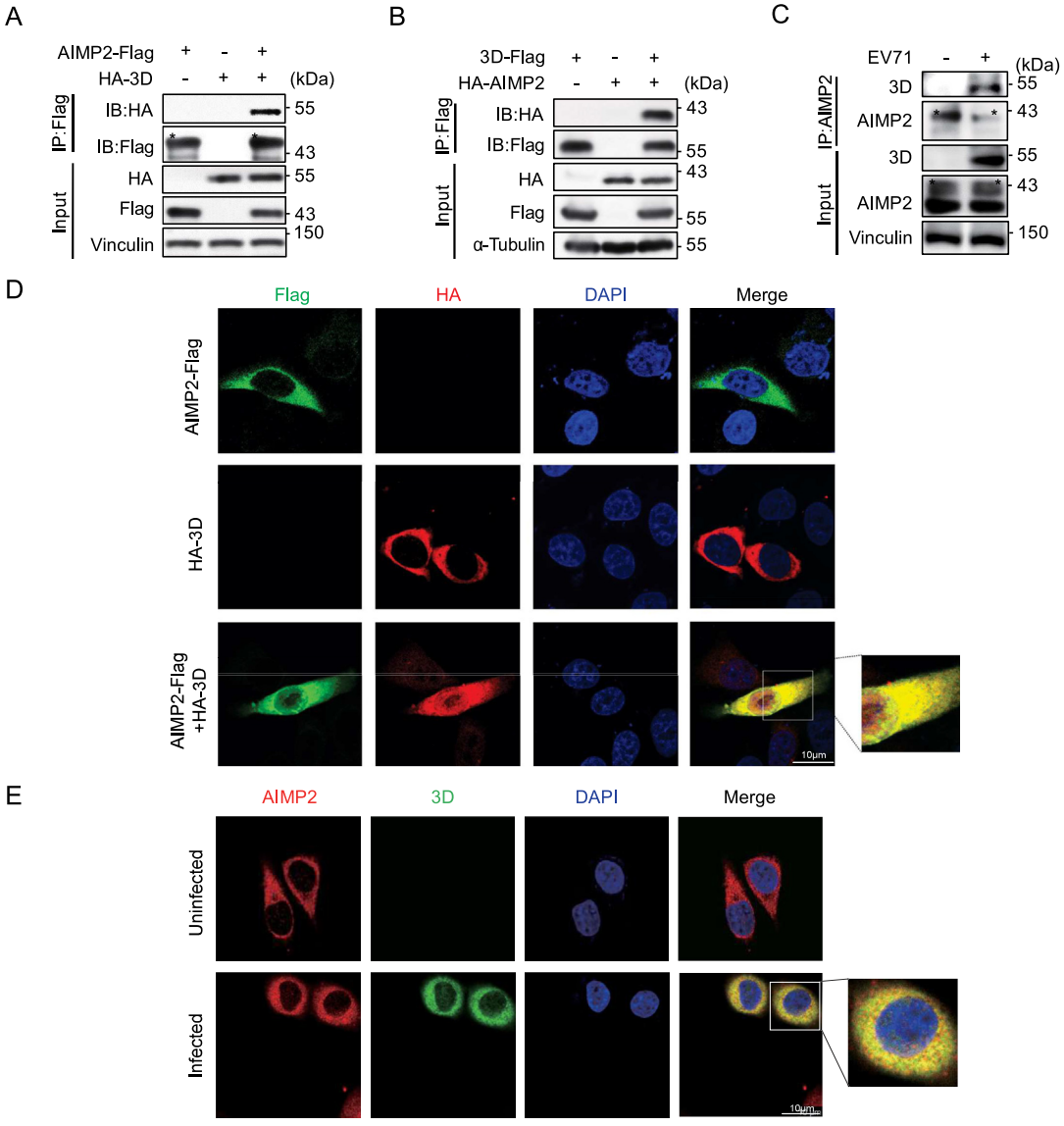

Fig. 5. AIMP2 interacts with EV71 3D polymerase. **A** HEK293T cells were transfected with the HA-3D plasmid alone, the AIMP2-Flag plasmid alone or HA-3D in combination with AIMP2-Flag. After 36 h of transfection, the cell lysates were immunoprecipitated with M2 beads and subjected to Western blot analysis with the indicated antibodies. **B** HEK293T cells were transfected with 3D-Flag alone, HA-AIMP2 alone or 3D-Flag in combination with HA-AIMP2. After 36 h of transfection, the cell lysates were subjected to immunoprecipitation with M2 beads, followed by Western blot analysis with the indicated antibodies. **C** RD cells were not infected (mock) or infected with EV71 (MOI = 1) for 12 h, and cell lysates were subjected to immunoprecipitation with an anti-AIMP2 antibody or control IgG, followed by Western blot analysis with the indicated antibodies. **D** HeLa cells were transfected with HA-3D alone, AIMP2-Flag alone or HA-3D in combination with AIMP2-Flag. After 36 h of transfection, the cells were treated with anti-Flag mouse antibody and anti-HA rabbit antibody overnight at 4 °C, and then incubated with Alexa Fluor 488 (green) and Alexa Fluor 555 (red). Nuclei were stained with DAPI (blue). Scale bars = 10 μm. **E** Endogenous colocalization between AIMP2 and the EV71 3D polymerase was detected in HeLa cells after 12 h of infection with EV71 (MOI = 1) by using anti-3D and anti-AIMP2 antibodies. Uninfected cells served as controls. Scale bars = 10 μm.

hypothesis, HEK293T cells were co-transfected with HA-3D and AIMP2-Flag plasmids. The Western blot results showed that AIMP2 degraded 3D polymerase in a dose-dependent manner (Fig. 6B). We also measured the mRNA level of 3D polymerase and found no effect (Fig. 6A). On the other hand, the HA-3D plasmid was transfected into HEK293T cells after knockdown of endogenous AIMP2. As expected, the immunoblot results indicated that knockdown of AIMP2 increased the protein level of 3D polymerase (Fig. 6C). In addition, we also investigated the effect of AIMP2 on the half-life of 3D polymerase. AIMP2-Flag and HA-3D plasmids were co-transfected into HEK293T cells. After 36 h of incubation, the cells were treated with CHX. The Western blot results revealed that AIMP2 reduced the half-life of 3D polymerase compared to the control group (Fig. 6D and E). In summary, AIMP2 reduces the stability of 3D polymerase.

To date, two main protein degradation pathways have been identified in eukaryotic cells: the ubiquitin-proteasome pathway and the autophagy-lysosome pathway (Rivett, 1990). Therefore, we further explored the mode of 3D polymerase degradation. First, HEK293T cells were

transfected with the HA-3D and AIMP2-Flag plasmids for 36 h and were then treated with the proteasome inhibitor MG132, lysosome inhibitor chloroquine (CQ) or autophagy inhibitor 3-methyladenine (3MA) for another 12 h. The immunoblot results suggested that after MG132 treatment, the reduction in 3D polymerase protein level was partially reversed (Fig. 6F). However, CQ (Fig. 6G) or 3MA (Fig. 6H) treatment did not rescue the degradation of 3D polymerase. In contrast, AIMP2 knockdown upregulated the expression of 3D polymerase. Compared to the NC group, the expression of 3D polymerase in MG132-treated group was significantly greater (Fig. 6I). These results demonstrate that AIMP2 mediates the degradation of the 3D polymerase via the ubiquitin-proteasome pathway.

To further verify the above results, we evaluated the effect of AIMP2 on 3D polymerase ubiquitination. HEK293T cells were transfected with the HA-AIMP2 and 3D-Flag plasmids for 36 h, and cell lysates were subjected to immunoprecipitation with M2 beads. Western blot results showed that the ubiquitin levels were significantly higher in cells co-transfected with AIMP2-Flag and HA-3D than in control cells (Fig. 6J). Taken together, these results demonstrate that AIMP2 increases the polyubiquitination of 3D polymerase and promotes its proteasome-mediated degradation.

Current studies indicate that K48-linked and K63-linked polyubiquitination are the two main types of polyubiquitination. Thus, we sought to determine which linkage of polyubiquitylation is present in 3D polymerase. To this end, HEK293T cells were transfected with the HA-3D and AIMP2-Flag plasmids together with the Ub-Myc (Fig. 6K), K48-Myc (Fig. 6L) or K63-Myc (Fig. 6M) plasmid, and the cell lysates were subjected to ubiquitination assay. The results suggest that AIMP2 can increase the ubiquitination of 3D polymerase via the K63 ubiquitin linkage but not the K48 ubiquitin linkage.

3.7. AIMP2 recruits the E3 ligase SMURF2 to promote the degradation of 3D polymerase

AIMP2 functions as a scaffold protein and mediates the degradation of 3D polymerase. Since AIMP2 is not an E3 ligase, we further explored the E3 ligases recruited by AIMP2 to target 3D polymerase. Kim et al. analyzed several E3 ligases that interact with AIMP2 (Kim et al., 2016), and Choi et al. reported that AIMP2 can interact with the E3 ligase TRAF2 (Choi et al., 2009a). We successfully constructed the E3 ligase plasmids CBL-Myc, TRAF3-Myc, TRAF2-Myc, SMURF2-Myc, ITCH-Myc and TRAF6-Myc, and then investigated whether the encoded ligases affect 3D polymerase stability. The results showed that AIMP2-mediated degradation of 3D polymerase was enhanced in the presence of the E3 ligase SMURF2 (Fig. 7A). We also verified the interaction between AIMP2 and SMURF2 (Fig. 7B). To further investigate the role of SMURF2, SMURF2 was knocked down in HEK293T cells, and the cells were transfected with the HA-3D and AIMP2-Flag plasmids for 36 h. The Western blot results showed that the inhibitory effect of AIMP2 on 3D polymerase expression was reversed after knockdown of endogenous SMURF2 (Fig. 7C). To further confirm that AIMP2 recruits SMURF2 to affect the stability of 3D polymerase, we knocked down endogenous AIMP2 in HEK293T cells, and then co-transfected the cells with HA-3D and SMURF2-Myc. The results suggested that the degradation of 3D polymerase was partially reversed after AIMP2 knockdown (Fig. 7D). Taken together, these results demonstrate that AIMP2 recruits the E3 ligase SMURF2 to promote the degradation of 3D polymerase.

Due to the recruitment of the E3 ligase SMURF2 by AIMP2 affecting the stability of 3D polymerase, we further investigated whether knocking down SMURF2 would affect EV71 infection. We knocked down SMURF2 in RD cells, transfected them with the AIMP2-Flag plasmid, and then the cells were infected with EV71 (MOI = 1). Immunoblot analysis was performed to detect viral proteins, and RT-qPCR was used to measure viral RNA levels. The results showed that knocking down SMURF2 rescued the inhibitory effect of AIMP2 on EV71 infection (Fig. 7E).

4. Discussion

Numerous studies in cancer and oncology research have demonstrate that AIMP2, a member of the AIMP family, serves as a tumor suppressor, primarily by regulating the polyubiquitination of target proteins (Zhou et al., 2020a, 2020b). Previous research has revealed that the interaction between AIMP2 and NS2 triggers a switch in the modification of M1, converting from ubiquitination to SUMOylation, thereby promoting influenza A virus replication (Gao et al., 2015). In this work, for the first time, we explored the role of AIMP2 in EV71 infection and found that AIMP2 overexpression inhibited EV71 replication and infection. Similarly, AIMP2 knockdown by siRNA promoted EV71 infection. In addition, we found that the inhibitory effect of AIMP2 on EV71 infection extends to other enterovirus serotypes, including CVA16 and CVB1 (Supplementary Fig. S1A and S1B). Given that CVA16 and EV71 are the primary causative pathogens of HFMD, AIMP2 may be useful as a novel therapeutic agent for HFMD.

Previous studies have demonstrated that host-mediated post-translational modifications play an important role in RNA virus pathogenesis (Kumar et al., 2020). For example, TRIM24 promotes cellular antiviral immunity by mediating K63-linked TRAF3 ubiquitination (Zhu et al., 2020); Cullin 4-mediated PB2 ubiquitination contributes to influenza A virus infection (Karim et al., 2020); and TRIM69 directly interacts with NS3 of dengue virus and mediates its polyubiquitination and degradation (Wang et al., 2018). Regarding the posttranslational modification of the EV71 3D polymerase, the acetylation of 3D polymerase has been demonstrated to enhance the binding affinity of 3D polymerase to viral RNA and promote viral proliferation (Hao et al., 2022). Moreover, SUMOylation of 3D polymerase can increase its stability and promote viral infection (Liu et al., 2016); in contrast, SUMOylation of 3C can inhibit viral infection (Chen et al., 2011). These findings suggest that posttranslational modifications of EV71 proteins are crucial for the antagonism between the host and the virus. Our study revealed that AIMP2 exerts antiviral effects by promoting polyubiquitination of 3D polymerase, and provided additional evidence that posttranslational modifications of 3D polymerase can affect viral infection. Moreover, the EV71 3D polymerase is an essential protein for enterovirus replication. Many current antienteroviral drugs target 3D polymerase to suppress viral replication and thereby hinder viral proliferation (Liu et al., 2023; Wang et al., 2023). Our work also identifies novel mechanisms that could be evaluated for the development of antienteroviral drugs.

Anti-restriction mechanisms have gradually evolved to allow viruses to counter host antagonism during viral infection. Recent studies have shown that the nonstructural protein 3C of EV71 functions as a protease capable of cleaving both EV71 precursor proteins and gasdermin D, thereby inhibiting pyroptosis (Lei et al., 2017). Enterovirus infection can induce RIG-I-mediated interferon responses. However, the protease activity of 3C reduces RIG-I expression, inhibiting the RIG-I signaling pathway and subsequently antagonizing the host's innate immune response (Xiao et al., 2021). Zhou et al. also reported that the 3C protease can cleave the host antiviral factor OAS3 and enhance viral replication (Zhou et al., 2022). In our study, AIMP2 was found to be degraded by the EV71 3C protein (Supplementary Fig. S2A and S2B). Therefore, we speculate that AIMP2 is similarly affected by the cleavage activity of 3C protease, and the precise mechanism is worth further exploration.

The process of viral replication is very complex, and our exploration focused solely on elucidating the regulatory mechanism of AIMP2 on 3D polymerase. Whether AIMP2 can affect other pathways in the replication step merits further investigation. In summary, our findings suggest that

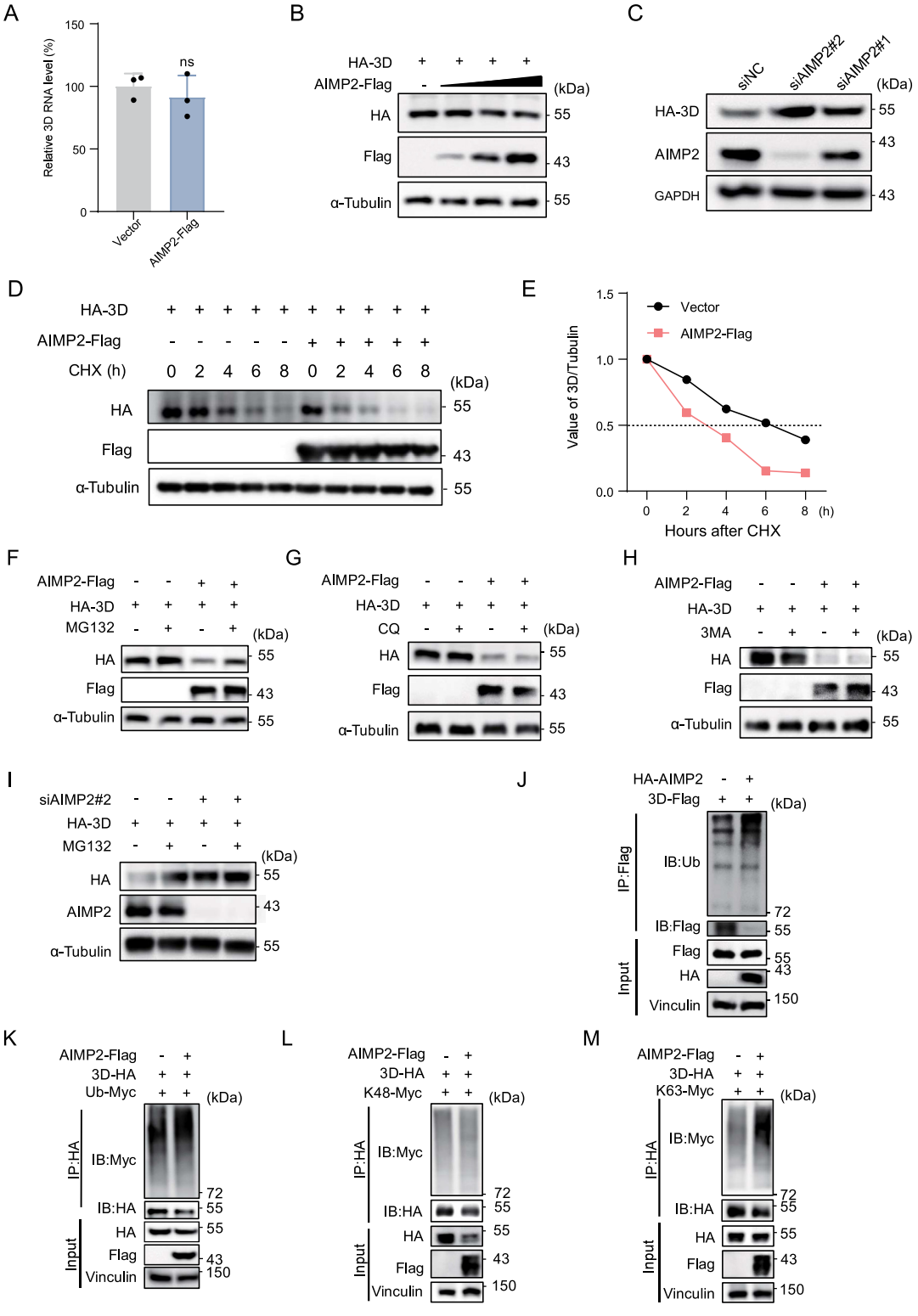

(caption on next page)

Fig. 6. AIMP2 degrades 3D polymerase through the ubiquitin-proteasome pathway. **A** HEK293T cells were transfected with the HA-3D and AIMP2-Flag plasmids for 36 h. The mRNA level of 3D polymerase was measured by RT-qPCR analysis. **B** HEK293T cells were transfected with the HA-3D and AIMP2-Flag plasmids (0, 0.5, 1, or 2 μg) for 36 h. The protein expression of 3D polymerase and AIMP2 was measured by immunoblotting with the indicated antibodies. **C** HEK293T cells were transfected with siRNA as indicated for 12 h and transfected with the HA-3D plasmid for another 36 h. The protein expression of 3D polymerase and AIMP2 was evaluated by immunoblotting with the indicated antibodies. **D, E** HEK293T cells transfected with AIMP2-Flag and HA-3D. After 36 h of incubation, the cells were treated with 100 μg/mL CHX for indicated time. The protein levels of HA-3D and AIMP2-Flag were analyzed by Western blot (**D**). The relative levels of HA-3D were quantified by signal intensity measurements and normalized to Tubulin levels (**E**). **F–H** HEK293T cells were transfected with the HA-3D and AIMP2-Flag plasmids for 36 h and treated with or without MG132 (20 μM) (**F**), chloroquine (CQ) (50 μM) (**G**) or 3MA (0.5 mM) (**H**) for 12 h. Then, the cells were lysed, and the protein expression of 3D and AIMP2 was analyzed by immunoblotting with the indicated antibodies. **I** HEK293T cells were transfected with siRNA as indicated for 12 h and were then transfected with the HA-3D plasmid for 24 h. Afterward, the cells were treated with MG132 for 12 h. The cells were lysed for immunoblotting with the indicated antibodies. **J** HEK293T cells were transfected with the 3D-Flag and HA-AIMP2 plasmids for 36 h and treated with MG132 (20 μM) for another 12 h, and the cell lysates were then subjected to immunoprecipitation with M2 beads and immunoblot analysis with an anti-ubiquitin antibody. **K–M** The Ub-Myc (**K**), K48-Myc (**L**) or K63-Myc (**M**) plasmid was transfected into HEK293T cells with AIMP2-Flag and HA-3D. The cell lysates were subjected to ubiquitination assay. The results represent the means ± SD from three independent experiments. Statistical significance was analyzed using Student's *t*-test (ns, not significant).

AIMP2 is released from the MSC complex upon EV71 infection to recruit the E3 ligase SMURF2, which promotes the K63-linked polyubiquitination of 3D polymerase and exerts antiviral effects. To counteract this host defense mechanism, the 3C protease potentially sustains viral infection by degrading the host protein AIMP2. In this study, we illustrate the dynamic regulatory mechanism of AIMP2 during EV71 infection. These findings are highly important for exploring the mechanism of 3D polymerase in EV71 replication and developing novel antiviral targets.

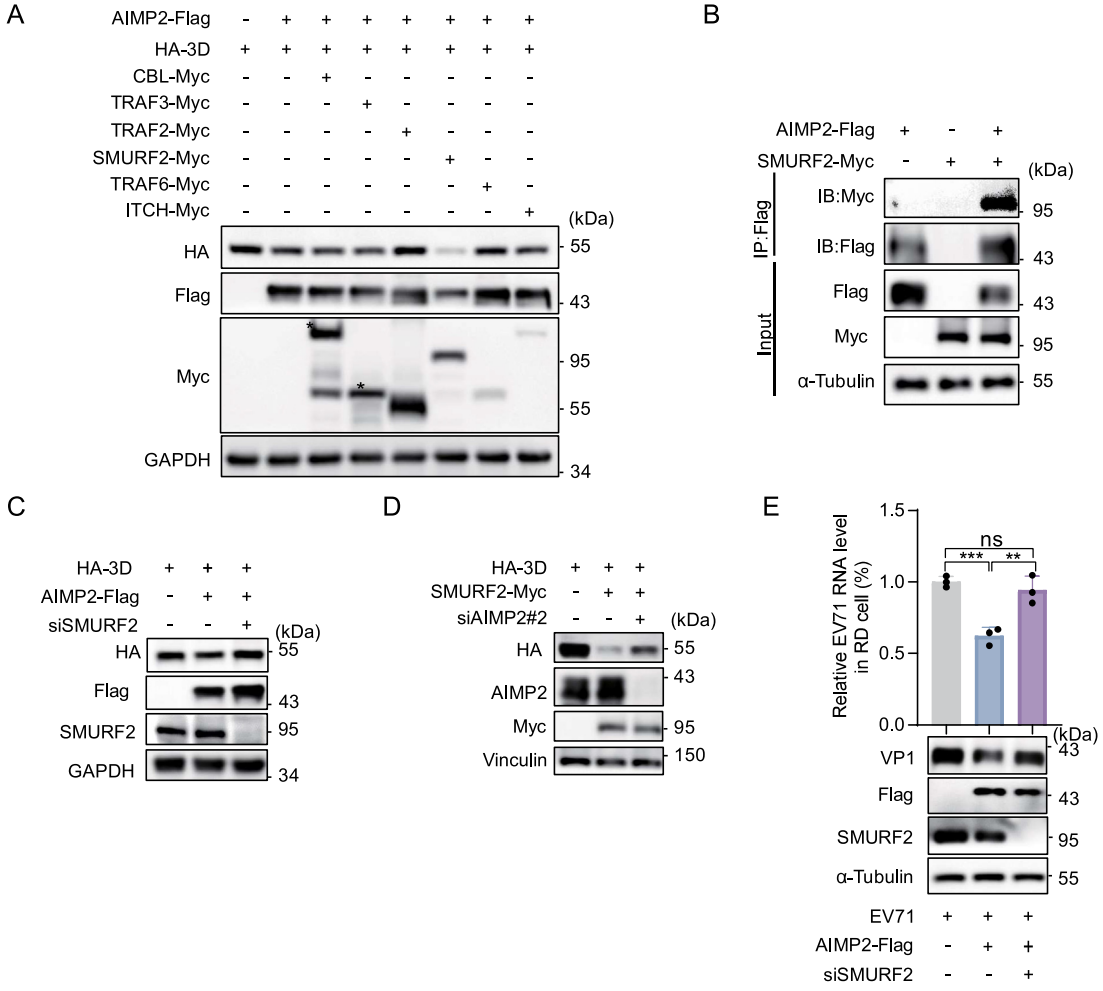

Fig. 7. AIMP2 recruits the E3 ligase SMURF2 to promote the degradation of 3D polymerase. **A** HEK293T cells were transfected with HA-3D, AIMP2-Flag and different E3 ligases expression plasmids. After 36 h, the cells were lysed and analyzed by Western blotting. **B** HEK293T cells were transfected with the SMURF2-Myc plasmid alone, the AIMP2-Flag plasmid alone or SMURF2-Myc in combination with AIMP2-Flag plasmid. After 36 h, the cell lysates were immunoprecipitated with M2 beads and subjected to Western blot analysis with the indicated antibodies. **C** HEK293T cells were transfected with siRNA as indicated for 12 h. Then, the cells were transfected with the HA-3D and AIMP2-Flag plasmids or the corresponding empty vector for 36 h, and the lysates were subjected to immunoblotting with the indicated antibodies. **D** HEK293T cells were transfected with siRNA as indicated for 12 h and were then cotransfected with HA-3D and SMURF2-Myc plasmids for 36 h. Cell lysates were subjected to Western blotting using the indicated antibodies. **E** After transfecting RD cells with specific siRNA for 12 h, followed by transfection with AIMP2-Flag for 24 h, the cells were infected with EV71 (MOI = 1). Subsequently, the protein levels were detected by Western blot, and the RNA levels were measured by RT-qPCR. The results represent the means ± SD from three independent experiments. Statistical significance was analyzed using Student's *t*-test (**$P < 0.01$, ***$P < 0.001$; ns, not significant).

5. Conclusions

In conclusion, our study demonstrates that the host protein AIMP2 exerts an antagonistic effect by recruiting the E3 ligase SMURF2 to promote the degradation of 3D polymerase, thereby inhibiting EV71 replication and weakening EV71 infectivity. At the same time, this antiviral effect also extends to the enterovirus serotypes CVA16 and CVB1. These findings provide a new target for the treatment of enteroviral infections and new insights for the development of antienteroviral drugs.

Data availability

All the data generated during the current study are included in the manuscript or supplementary information.

Ethics statement

This study does not contain any studies with human or animal objects by any of the authors.

Author contributions

Junrui Ren: designed and performed the experiments, data analysis, writing original draft. Lei Yu: methodology, performed the experiments and edited draft. Qiuhan Zhang: methodology and prepared the EV71 virus. Pengyu Ren: performed the experiments. Yumeng Cai: formal analysis. Xueyun Wang: investigation. Ke Lan: contributed to project administration, supervision, editing the draft and funding acquisition. Shuwen Wu: contributed to project administration, supervision, data curation, editing the draft and funding acquisition. All authors read and approved the manuscript.

Conflict of interest

Prof. Ke Lan is an editorial board member for *Virologica Sinica* and was not involved in the editorial review or the decision to publish this article. The authors declare that they have no conflicts of interest.

Acknowledgements

We thank Dr. Bo Zhang (Wuhan Institution of Virology, CAS) for generously providing pACYC-EV-A71-FL plasmid. This work was supported by National Natural Science Foundation of China (32188101 and 81971976).

Appendix A. Supplementary data

Supplementary data to this article can be found online at https://doi.org/10.1016/j.virs.2024.06.009.

References

Ang, P.Y., Chong, C.W.H., Alonso, S., 2021. Viral determinants that drive Enterovirus-A71 fitness and virulence. Emerg. Microbes Infect. 10, 713–724.
Baer, A., Kehn-Hall, K., 2014. Viral concentration determination through plaque assays: using traditional and novel overlay systems. J. Vis. Exp., e52065
Baggen, J., Thibaut, H.J., Strating, J., van Kuppeveld, F.J.M., 2018. The life cycle of non-polio enteroviruses and how to target it. Nat. Rev. Microbiol. 16, 368–381.
Chen, S.C., Chang, L.Y., Wang, Y.W., Chen, Y.C., Weng, K.F., Shih, S.R., Shih, H.M., 2011. Sumoylation-promoted enterovirus 71 3C degradation correlates with a reduction in viral replication and cell apoptosis. J. Biol. Chem. 286, 31373–31384.
Choi, J.W., Kim, D.G., Park, M.C., Um, J.Y., Han, J.M., Park, S.G., Choi, E.C., Kim, S., 2009a. AIMP2 promotes TNFalpha-dependent apoptosis via ubiquitin-mediated degradation of TRAF2. J. Cell Sci. 122, 2710–2715.
Choi, J.W., Um, J.Y., Kundu, J.K., Surh, Y.J., Kim, S., 2009b. Multidirectional tumor-suppressive activity of AIMP2/p38 and the enhanced susceptibility of AIMP2 heterozygous mice to carcinogenesis. Carcinogenesis 30, 1638–1644.
Cox, B., Levent, F., 2018. Hand, foot, and mouth disease. JAMA 320, 2492.
Gao, S., Wu, J., Liu, R.Y., Li, J., Song, L., Teng, Y., Sheng, C., Liu, D., Yao, C., Chen, H., Jiang, W., Chen, S., Huang, W., 2015. Interaction of NS2 with AIMP2 facilitates the switch from ubiquitination to SUMOylation of M1 in influenza A virus-infected cells. J. Virol. 89, 300–311.
Guo, H., Li, Y., Liu, G., Jiang, Y., Shen, S., Bi, R., Huang, H., Cheng, T., Wang, C., Wei, W., 2019. A second open reading frame in human enterovirus determines viral replication in intestinal epithelial cells. Nat. Commun. 10, 4066.
Hagiwara, A., Yoneyama, T., Takami, S., Hashimoto, I., 1984. Genetic and phenotypic characteristics of enterovirus 71 isolates from patients with encephalitis and with hand, foot and mouth disease. Arch. Virol. 79, 273–283.
Han, J.M., Park, B.J., Park, S.G., Oh, Y.S., Choi, S.J., Lee, S.W., Hwang, S.K., Chang, S.H., Cho, M.H., Kim, S., 2008. AIMP2/p38, the scaffold for the multi-tRNA synthetase complex, responds to genotoxic stresses via p53. Proc. Natl. Acad. Sci. USA 105, 11206–11211.
Hao, H., Liu, W., Miao, Y., Ma, L., Yu, B., Liu, L., Yang, C., Zhang, K., Chen, Z., Yang, J., Zheng, Z., Zhang, B., Deng, F., Gong, P., Yuan, J., Hu, Z., Guan, W., 2022. N4-acetylcytidine regulates the replication and pathogenicity of enterovirus 71. Nucleic Acids Res. 50, 9339–9354.
Hu, Y., Jiang, L., Peng, H.L., 2015. Clinical analysis of 134 children with nervous system damage caused by enterovirus 71 infection. Pediatr. Infect. Dis. J. 34, 718–723.
Karim, M., Biquand, E., Declercq, M., Jacob, Y., van der Werf, S., Demeret, C., 2020. Nonproteolytic K29-linked ubiquitination of the PB2 replication protein of influenza A viruses by proviral cullin 4-based E3 ligases. mBio 11, e00305–e00320.
Kim, D.G., Lee, J.Y., Lee, J.H., Cho, H.Y., Kang, B.S., Jang, S.Y., Kim, M.H., Guo, M., Han, J.M., Kim, S.J., Kim, S., 2016. Oncogenic mutation of AIMP2/p38 inhibits its tumor-suppressive interaction with Smurf2. Cancer Res. 76, 3422–3436.
Kim, S.S., Hur, S.Y., Kim, Y.R., Yoo, N.J., Lee, S.H., 2011. Expression of AIMP1, 2 and 3, the scaffolds for the multi-tRNA synthetase complex, is downregulated in gastric and colorectal cancer. Tumori 97, 380–385.
Kumar, R., Mehta, D., Mishra, N., Nayak, D., Sunil, S., 2020. Role of host-mediated post-translational modifications (PTMs) in RNA virus pathogenesis. Int. J. Mol. Sci. 22, 323.
Lei, X., Zhang, Z., Xiao, X., Qi, J., He, B., Wang, J., 2017. Enterovirus 71 inhibits pyroptosis through cleavage of gasdermin D. J. Virol. 91, e01069-17.
Li, M.L., Brewer, G., 2020. Functional analyses of mammalian virus 5'UTR-derived, small RNAs that regulate virus translation. Methods 183, 13–20.
Lin, J.Y., Li, M.L., Shih, S.R., 2009. Far upstream element binding protein 2 interacts with enterovirus 71 internal ribosomal entry site and negatively regulates viral translation. Nucleic Acids Res. 37, 47–59.
Liu, X., Xu, Z., Liang, J., Yu, L., Ren, P., Zhou, H.B., Wu, S., Lan, K., 2023. Identification of a novel acylthiourea-based potent broad-spectrum inhibitor for enterovirus 3D polymerase in vitro and in vivo. Antiviral Res. 213, 105583.
Liu, Y., Zheng, Z., Shu, B., Meng, J., Zhang, Y., Zheng, C., Ke, X., Gong, P., Hu, Q., Wang, H., 2016. SUMO modification stabilizes enterovirus 71 polymerase 3D to facilitate viral replication. J. Virol. 90, 10472–10485.
Lulla, V., Dinan, A.M., Hosmillo, M., Chaudhry, Y., Sherry, L., Irigoyen, N., Nayak, K.M., Stonehouse, N.J., Zilbauer, M., Goodfellow, I., Firth, A.E., 2019. An upstream protein-coding region in enteroviruses modulates virus infection in gut epithelial cells. Nat. Microbiol. 4, 280–292.
Nechushtan, H., Kim, S., Kay, G., Razin, E., 2009. Chapter 1: The physiological role of lysyl tRNA synthetase in the immune system. Adv. Immunol. 103, 1–27.
Ofir-Birin, Y., Fang, P., Bennett, S.P., Zhang, H.M., Wang, J., Rachmin, I., Shapiro, R., Song, J., Dagan, A., Pozo, J., Kim, S., Marshall, A.G., Schimmel, P., Yang, X.L., Nechushtan, H., Razin, E., Guo, M., 2013. Structural switch of lysyl-tRNA synthetase between translation and transcription. Mol. Cell 49, 30–42.
Ooi, M.H., Wong, S.C., Lewthwaite, P., Cardosa, M.J., Solomon, T., 2010. Clinical features, diagnosis, and management of enterovirus 71. Lancet Neurol. 1097–1105.
Rivett, A.J., 1990. Eukaryotic protein degradation. Curr. Opin. Cell Biol. 2, 1143–1149.
Saguil, A., Kane, S.F., Lauters, R., Mercado, M.G., 2019. Hand-Foot-and-Mouth disease: rapid evidence review. Am. Fam. Physician 100, 408–414.
Schmidt, N.J., Lennette, E.H., Ho, H.H., 1974. An apparently new enterovirus isolated from patients with disease of the central nervous system. J. Infect. Dis. 129, 304–309.
Shang, B., Deng, C., Ye, H., Xu, W., Yuan, Z., Shi, P.Y., Zhang, B., 2013. Development and characterization of a stable eGFP enterovirus 71 for antiviral screening. Antiviral Res. 97, 198–205.
Shih, S.R., Stollar, V., Li, M.L., 2011. Host factors in enterovirus 71 replication. J. Virol. 85, 9658–9666.
Shin, J.Y., Lee, B., Ham, S., Kim, J.H., Kim, H., Kim, H., Jo, M.G., Kim, H.J., Park, S.W., Kweon, H.S., Kim, Y.J., Yun, S.P., Lee, Y., 2022. Pharmacological inhibition of AIMP2 aggregation attenuates α-synuclein aggregation and toxicity in Parkinson's disease. Biomed. Pharmacother. 156, 113908.
Solomon, T., Lewthwaite, P., Perera, D., Cardosa, M.J., McMinn, P., Ooi, M.H., 2010. Virology, epidemiology, pathogenesis, and control of enterovirus 71. Lancet Infect. Dis. 10, 778–790.
Tang, Q., Li, S., Du, L., Chen, S., Gao, J., Cai, Y., Xu, Z., Zhao, Z., Lan, K., Wu, S., 2020. Emetine protects mice from enterovirus infection by inhibiting viral translation. Antiviral Res. 173, 104650.
Wang, H., Li, Y., 2019. Recent progress on functional genomics research of enterovirus 71. Virol. Sin. 34, 9–21.
Wang, K., Zou, C., Wang, X., Huang, C., Feng, T., Pan, W., Wu, Q., Wang, P., Dai, J., 2018. Interferon-stimulated TRIM69 interrupts dengue virus replication by ubiquitinating viral nonstructural protein 3. PLoS Pathog. 14, e1007287.
Wang, X., Hu, Z., Zhang, W., Wu, S., Hao, Y., Xiao, X., Li, J., Yu, X., Yang, C., Wang, J., Zhang, H., Ma, F., Shi, W., Wang, J., Lei, X., Zhang, X., He, S., 2023. Inhibition of

lysosome-tethered Ragulator-Rag-3D complex restricts the replication of Enterovirus 71 and Coxsackie A16. J. Cell Biol. 222, e202303108.
Xia, H., Wang, P., Wang, G.C., Yang, J., Sun, X., Wu, W., Qiu, Y., Shu, T., Zhao, X., Yin, L., Qin, C.F., Hu, Y., Zhou, X., 2015. Human enterovirus nonstructural protein 2CATPase functions as both an RNA helicase and ATP-independent RNA chaperone. PLoS Pathog. 11, e1005067.
Xiao, H., Li, J., Yang, X., Li, Z., Wang, Y., Rui, Y., Liu, B., Zhang, W., 2021. Ectopic expression of TRIM25 restores RIG-I expression and IFN production reduced by multiple enteroviruses 3C(pro). Virol. Sin. 36, 1363–1374.
You, Q., Wu, J., Liu, Y., Zhang, F., Jiang, N., Tian, X., Cai, Y., Yang, E., Lyu, R., Zheng, N., Chen, D., Wu, Z., 2023. HMGB1 release induced by EV71 infection exacerbates blood-brain barrier disruption via VE-cadherin phosphorylation. Virus Res. 338, 199240.
Yuan, J., Shen, L., Wu, J., Zou, X., Gu, J., Chen, J., Mao, L., 2018. Enterovirus A71 proteins: structure and function. Front. Microbiol. 9, 286.
Yum, M.K., Kang, J.S., Lee, A.E., Jo, Y.W., Seo, J.Y., Kim, H.A., Kim, Y.Y., Seong, J., Lee, E.B., Kim, J.H., Han, J.M., Kim, S., Kong, Y.Y., 2016. AIMP2 controls intestinal stem cell compartments and tumorigenesis by modulating Wnt/β-catenin signaling. Cancer Res. 76, 4559–4568.
Zhang, H., Song, L., Cong, H., Tien, P., 2015. Nuclear protein Sam68 interacts with the enterovirus 71 internal ribosome entry site and positively regulates viral protein translation. J. Virol. 89, 10031–10043.
Zhang, Q., Li, S., Lei, P., Li, Z., Chen, F., Chen, Q., Wang, Y., Gong, J., Tang, Q., Liu, X., Lan, K., Wu, S., 2021. ANXA2 facilitates enterovirus 71 infection by interacting with 3D polymerase and PI4KB to assist the assembly of replication organelles. Virol. Sin. 36, 1387–1399.
Zhou, X., Tian, L., Wang, J., Zheng, B., Zhang, W., 2022. EV71 3C protease cleaves host anti-viral factor OAS3 and enhances virus replication. Virol. Sin. 37, 418–426.
Zhou, Z., Sun, B., Huang, S., Yu, D., Zhang, X., 2020a. Roles of aminoacyl-tRNA synthetase-interacting multi-functional proteins in physiology and cancer. Cell Death Dis. 11, 579.
Zhou, Z., Sun, B., Nie, A., Yu, D., Bian, M., 2020b. Roles of aminoacyl-tRNA synthetases in cancer. Front. Cell Dev. Biol. 8, 599765.
Zhu, Q., Yu, T., Gan, S., Wang, Y., Pei, Y., Zhao, Q., Pei, S., Hao, S., Yuan, J., Xu, J., Hou, F., Wu, X., Peng, C., Wu, P., Qin, J., Xiao, Y., 2020. TRIM24 facilitates antiviral immunity through mediating K63-linked TRAF3 ubiquitination. J. Exp. Med. 217, e20192083.